coatings

MDPI

Article

Experimental Study on Preparation of Tungsten-Carbide-Particle-Reinforced Nickel-Based Alloy Plasma Surfacing Layer on Descaling Roller Surface

Lei Feng [1,†], Chang Li [1,*,†], Xing Han [1], Fenghua Luo [2] and Han Sun [1]

[1] College of Mechanical Engineering and Automation, University of Science and Technology Liaoning, Anshan 114051, China
[2] State Key Laboratory of Powder Metallurgy, Central South University, Changsha 410083, China
* Correspondence: lichang2323-23@163.com
† These authors are co-first authors of the article.

Abstract: The descaling roller is a significant component in steel rolling production. Under harsh service conditions, the descaling roller is subjected to the dynamic impact caused by high-pressure water erosion and a high-temperature billet descaling process for a long time. Under the harsh conditions of high temperature, strong wear, multi-cycle heat, force, flow, and multi-field strong coupling, the roller surface is prone to wear and corrosion failure, which affects the production cost and efficiency. Through plasma surfacing technology, a high-performance coating can be applied on the conventional metal surface to effectively improve its surface properties. It is important to carry out experimental research on the surface plasma surfacing of the descaling roller to prolong product life, improve product quality, and save cost. At present, the research on the 42CrMo scaler matrix plasma surfacing of nickel-based alloys with different WC contents is still lacking. In this paper, 70%NiCrBSi+30%WC powder and 40%NiCrBSi+60%WC powder were used as surfacing materials; plasma surfacing experiments were carried out on the 42CrMo matrix; and SEM, XRD, microhardness, friction and wear, and corrosion tests were carried out on the surfacing layer to evaluate the feasibility of preparing an ultra-high-hardness WC-particle-reinforced nickel-based alloy plasma surfacing layer on the descaling roller surface and to explore the WC hard phase dissolution behavior and complex secondary phase formation mechanism. The results show that γ(Fe/Ni), Fe-Ni, FeSi, Fe_3C, and M_7C_3 are the main phases in the Ni/WC plasma surfacing layer. The diffusion and precipitation of elements occur in the molten pool, and complex secondary phases are formed in the surfacing layer. Compared with the 70%NiCrBSi+30%WC surfacing layer, the WC deposition phenomenon of the 40%NiCrBSi+60%WC surfacing layer has been significantly improved and has better hardness, wear resistance, and corrosion resistance. Based on the welding test, the correlation law between powder formulation, welding structure, and surfacing layer properties was revealed in this study, which lays a theoretical foundation for the preparation of high-performance coating on the descaling roller surface and has significant engineering application value and practical significance.

Keywords: descaling roller; plasma surfacing welding; nickel-based WC powder; material characterization experiment; WC dissolution and diffusion behavior

Citation: Feng, L.; Li, C.; Han, X.; Luo, F.; Sun, H. Experimental Study on Preparation of Tungsten-Carbide-Particle-Reinforced Nickel-Based Alloy Plasma Surfacing Layer on Descaling Roller Surface. *Coatings* **2024**, *14*, 729. https://doi.org/10.3390/coatings14060729

Academic Editor: Hideyuki Murakami

Received: 9 May 2024
Revised: 29 May 2024
Accepted: 30 May 2024
Published: 6 June 2024

1. Introduction

The descaling roller is a key component in the field of iron and steel metallurgy. It has been subjected to high-pressure water erosion and high-temperature billet dynamic impact for a long time. Under the action of high temperature, strong wear, and multi-cycle thermo-force-flow multi-field strong coupling, the surface is prone to wear and corrosion. The continued use of the damaged descaling roller will affect the product quality, and descaling roller replacement will require a variety of human, material, and financial resources, which will seriously affect the cost and efficiency of the production [1,2].

Through additive manufacturing, high-performance coatings are prepared on conventional metal surfaces, which can effectively improve the surface properties. The preparation of high-performance surface coatings can effectively repair and strengthen the part surface properties and improve their cost performance [3]. Common surface processes include laser cladding, supersonic spraying, and plasma surfacing [4,5]. Plasma surfacing has a flat pass advantage, uniform structure, fewer defects, energy concentration, base metal dilution rate, and small heat-affected zone [6], and its principle is shown in Figure 1. Plasma surfacing is a welding method that uses a plasma arc as a heat source, fills metal alloy powder or welding wire, forms a molten pool on the workpiece surface, and obtains a good-performance surfacing layer after cooling.

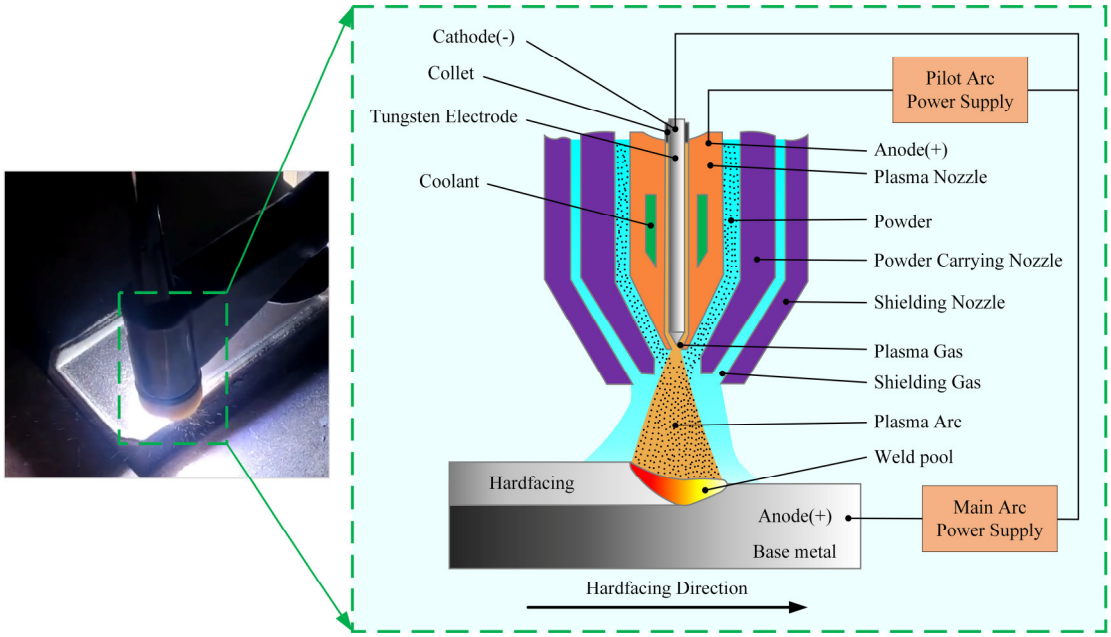

Figure 1. Schematic of plasma surfacing welding.

In engineering applications, Ni-Cr-B-Si alloy powder is often used for plasma surfacing, and the surfacing layer has great wear resistance and corrosion resistance [7]. Sudha et al. [8] used surfacing nickel-based wear-resistant alloy on a 304 L stainless steel surface via plasma surfacing and found that the hardness was as high as 700 HV in the area rich in a large number of acicular structures in the chromium compounds. Kesavan et al. [9] studied the high-temperature wear performance of the nickel-based surfacing layer and found that the wear resistance increased with the increase in temperature, and the wear resistance of the surfacing layer was the best at a temperature of 823 K. Sreevidya N et al. [10] analyzed the effect of the dilution rate on the high-temperature and high-vacuum friction properties of the stainless steel plasma transfer arc welding Ni-Cr-B-Si coating. The coatings with different dilution rates were prepared via different welding currents. It was found that with the increase in dilution rate, the microstructure changed from hypereutectic to eutectic, and the distribution and content of borides and carbides changed. Kumar et al. [11] prepared a Ni-based surfacing alloy coating on the surface of 316 LN stainless steel via the plasma transfer arc welding process, analyzed the coating wear behavior, characterized its microstructure and hardness, and concluded that adhesive wear was the main wear mechanism.

Many studies have shown that nickel-based alloy surfacing layer has great performance. However, the practice has proved that the simple nickel-based alloy surfacing welding cannot meet the requirements of wear resistance and corrosion resistance on the descaling roller. Therefore, researchers have developed a composite reinforcement material composed of a metal system with great ductility and a hard and brittle ceramic phase, namely, a metal-based ceramic composite [12]. It uses metal materials with great heat

resistance and ductility to bond ceramics with high hardness and brittleness together and uses a high-hardness ceramic phase to resist repeated friction and wear of parts during the service process. Under the impact of external force, the metal with great ductility can provide buffer space for plastic deformation in the hard phase of the ceramic and absorb part of the energy, giving full play to the great plasticity in the metal alloy powder and the high hardness of the ceramic phase so that the coating has both great toughness and high hardness [13,14]. Metal-based ceramic composites are far superior to traditional metal alloy coatings in terms of performance and are widely used in the surface repair and protection of parts [15,16]. In engineering applications, the WC hard phase is usually added to nickel-based alloys, which is because nickel-based alloys have great wettability to WC, and WC itself has the advantages of high hardness, high melting point, and great weldability. A WC hard-phase-reinforced nickel-based alloy surfacing layer has better performance than a single nickel-based alloy surfacing layer, and many scholars have conducted a variety of research on this subject.

Wei et al. [17] prepared a nickel-based composite coating with high WC content via plasma transfer arc (PTA) surface-welding and optimized the welding parameters of Ni-based WC composite coating via an orthogonal test. The results show that welding current, powder feeding rate, and welding speed have significant effects on WC dissolution. The optimal surfacing current, powder feeding rate, and welding speed are 100 A, 25 g/min, and 40 mm/min, respectively. Wang W et al. [18] prepared an iron-based WC coating on the Al6061 matrix and analyzed the effects of different sizes of WC (80 μm, 55 μm, and 3.5 μm) on the microstructure and coating wear resistance. The results show that the microhardness of the coating increases with the increase in WC particle size, and the WC-Fe composite coating (55 μm) shows the best wear resistance. Appiah A et al. [19] used plasma surfacing welding to prepare Ni-based WC coatings with WC contents of 45% and 60%, respectively, on the structural steel surface. They found that the hard phase of the coating is mainly WC and secondary carbides. The Cr content increase can improve the wear resistance of the coating, and the wear resistance of the coating increases with the increase in WC addition. Adamiak M et al. [20] prepared NiSiB+60%WC alloy powder on a structural steel matrix through laser cladding (LC) and plasma powder transfer arc welding (PPTAW). The results show that both methods lead to the precipitation of a secondary WC phase during solidification, but the cladding layer of PPTAW shows a dendrite structure. The microhardness of the cladding prepared via the two methods is similar, but the wear resistance of PPTAW cladding is better than that of LC cladding. Both methods cause the cladding layer and matrix to form metallurgical bonding, but the dilution rate of the LC method is lower. Compared with the heat-affected zone of PPTAW coating, the HAZ of the LC process is larger. Yi J et al. [21] used plasma transfer arc welding (PTA) to prepare the cladding layer with micro- and nano-sized WC. The effect of WC size on microstructure evolution and wear performance was analyzed. The study shows that the nano-WC particle coating exhibits more fine grains and nanoparticles.

The above research shows that the WC-hard-phase-reinforced nickel-based alloy surfacing layer has excellent performance and wide application prospects. However, in engineering practice, the surface plasma surfacing of Ni-based WC is often affected by unreasonable powder composition selection and a mismatch of process parameters, and the surfacing layer is prone to cracking and poor weldability. Therefore, it is important to carry out experimental research on plasma surfacing of Ni-based alloy powder with different WC contents on the descaling roller surface and explore its welding mechanism. At present, the research on the 42CrMo scaler matrix plasma surfacing of nickel-based alloys with different WC contents is still lacking; only basic research on the internal metallurgical mechanism during welding has been undertaken. In this paper, 70%NiCrBSi+30%WC powder and 40%NiCrBSi+60%WC powder were used as surfacing materials; plasma surfacing experiments were carried out on 42CrMo matrix; and SEM, XRD, microhardness, friction and wear, and corrosion tests were carried out on the surfacing layer to evaluate the feasibility of preparing ultra-high-hardness WC-particle-reinforced nickel-based alloy

plasma surfacing layer on the descaling roller surface and to explore the WC hard phase dissolution behavior and complex secondary phase formation mechanism. Based on the welding test, the correlation law between powder formulation, welding structure, and surfacing layer properties was revealed in this study, which lays a theoretical foundation for the preparation of high-performance coating on the descaling roller surface and has significant engineering application value and practical significance.

2. Plasma Surfacing Welding Experiment

2.1. Experimental Materials

The experiment is based on the 42CrMo descaling roller of China Zhengfa Company for plasma surfacing welding. The composition information and mechanical properties of 42CrMo are provided by the factory, as shown in Tables 1 and 2, respectively.

Table 1. Composition and content of 42CrMo (wt%).

Element	Ni	Mo	Cr	Mn	Si	C	P	S	Fe
Content (wt%)	0.04	0.21	0.98	0.77	0.15	0.37	0.03	0.04	Bal.

Table 2. Mechanical properties of 42CrMo.

Temperature/°C	Young's Modulus/Gpa	Yield Strength/Mpa
20	210	930
100	205	895
200	185	850
300	175	780
400	165	700

The surfacing powder material was self-prepared 70%NiCrBSi+30%WC and 40%NiCrBSi+60%WC self-fusible nickel-based alloy composite powder. Among these, the purity of NiCrBSi powder is 99%, and the purity of WC powder is 99.5%. Both are produced by China Zhengfa Company. The elemental content of the nickel-based alloy powder is shown in Table 3. The elemental content of WC powder is shown in Table 4. The weight of the nickel-based alloy powder and the WC alloy powder required by the two composite powders were accurately weighed by an electronic balance and then added into the ball mill tank together with the weight, without adding the ball mill ball and without adding anhydrous ethanol. An angle of 60 to 80° was set, and the substances were mixed for 10 h at a speed of 300 rpm. Finally, a vacuum drying box was used to dry the mixed powder, with a drying time of 10 h at a drying temperature of 65 °C.

Table 3. Nickel-based elemental composition.

Element	C	Si	B	Cr	Fe	Ni
Content(wt%)	0.3	3.3	1.7	8	2.3	Bal.

Table 4. WC elemental composition.

Element	C	W
Content (wt%)	6.0	Bal.

The microstructure and phase analysis of the mixed Ni-based WC powder were investigated with a Sigma500 field emission scanning electron microscope (SEM), an Energy Dispersive Spectroscopy (EDS), and an X-ray diffractometer (XRD). In this experiment, the Sigma 500 scanning electron microscope produced by Carl Zeiss AG (Carl Zeiss AG, Oberkochen, Germany) was used to observe the microstructure. During the experiment, the acceleration voltage was set to 15 kV and the SE2 scanning probe was used with a scanning

focal length range of 8~12 mm. EDS was performed with the XFlash 6 | 100 detector of BRUKER, karlsruhe, Germany, to obtain the element distribution and composition information of the sample. XRD equipment produced by PANalytical B.V (PANalytical B.V, Almelo, Netherlands) in the Netherlands was used for an X-ray diffractometer experiment to analyze the phase composition of the surfacing layer. The device uses Kα as the ray source, and the target material is Cu. In the process of the experiment, the scanning angle was 20°~90° and the scanning time was 2 min.

The microscopic morphology and elemental distribution of 70%NiCrBSi+30%WC powder are shown in Figure 2, and the microscopic morphology and elemental distribution of 40%NiCrBSi+60%WC powder are shown in Figure 3. In the figure, the nickel-based alloy powder is spherical, and the WC powder is irregular stone. The irregular WC particles in 70%NiCrBSi+30%WC were significantly fewer than those in 40%NiCrBSi+60%WC particles. The WC particles are evenly distributed in the mixed powder, indicating that the mixing effect in the preparation of nickel-based WC powder is better. The particle sizes of NiCrBSi powder and WC powder were statistically analyzed via scanning electron microscopy results and data processing software, and the results are shown in Figure 4. Among them, the particle size of NiCrBSi powder is in the range of 30 μm~170 μm, and the average particle size is 79.6 μm. The particle size of WC powder is in the range of 65 μm~235 μm, and the average particle size is 139.38 μm. The XRD analysis results of the two alloy powders are shown in Figure 5. WC, W_2C, SiC, γ-(Ni, Fe), CrSi, MnB_2, and other elements and their compounds were detected in the powders. The peak value of γ-Ni was the highest in 70%NiCrBSi+30%WC powder, while the peak value of W_2C was the highest in 40%NiCrBSi+60%WC powder. It shows that the phase and peak intensity of the highest peak have obviously changed due to the WC content difference.

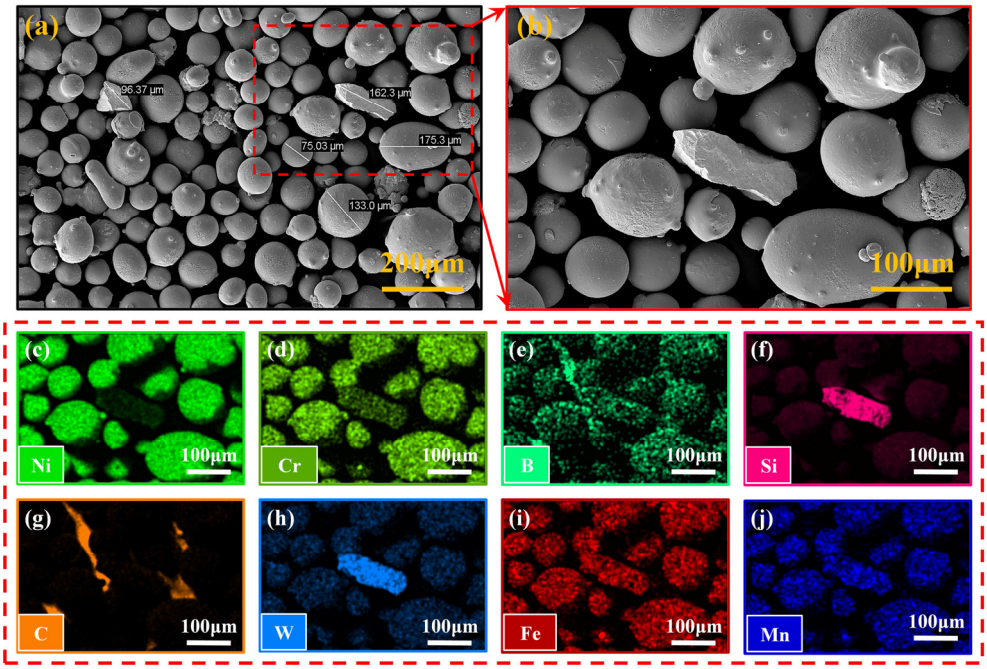

Figure 2. SEM and EDS results of 70%NiCrBSi+30%WC powder: (**a**) 100× SEM results of 70%NiCrBSi+30%WC powder; (**b**) local magnification of 70%NiCrBSi+30%WC SEM; (**c**–**j**) the EDS element surface scan result of Ni, Cr, B, Si, C, W, Fe, and Mn, corresponding to view (**b**).

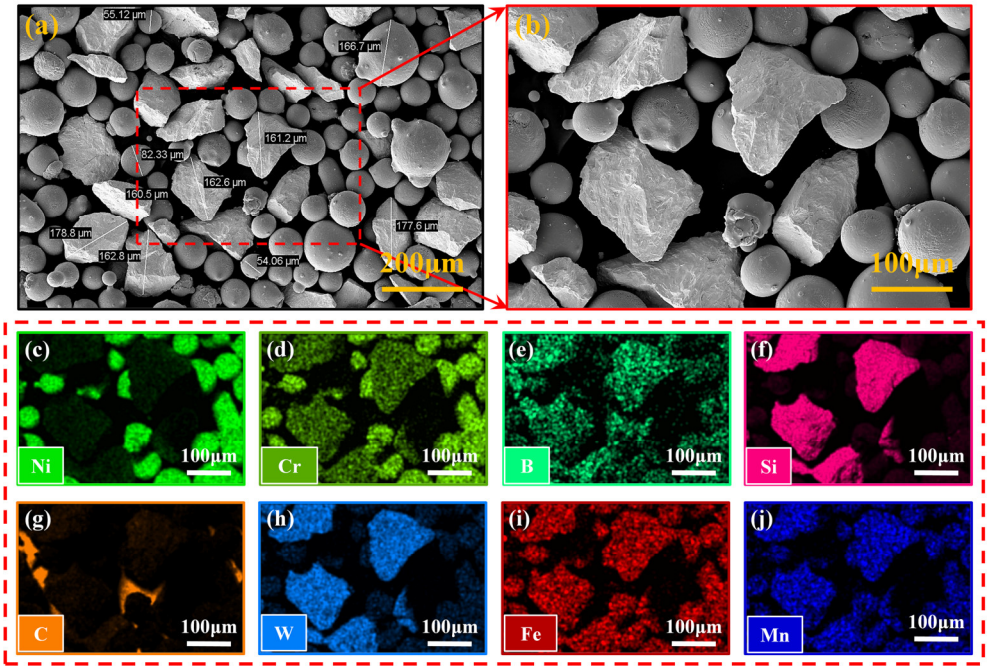

Figure 3. SEM results and EDS results of 40%NiCrBSi+60%WC powder: (**a**) SEM results of 40%NiCrBSi+60%WC 100 times; (**b**) SEM local magnification of 40%NiCrBSi+60%WC powder; (**c**–**j**) the EDS element surface scan results of Ni, Cr, B, Si, C, W, Fe, and Mn, corresponding to view (**b**).

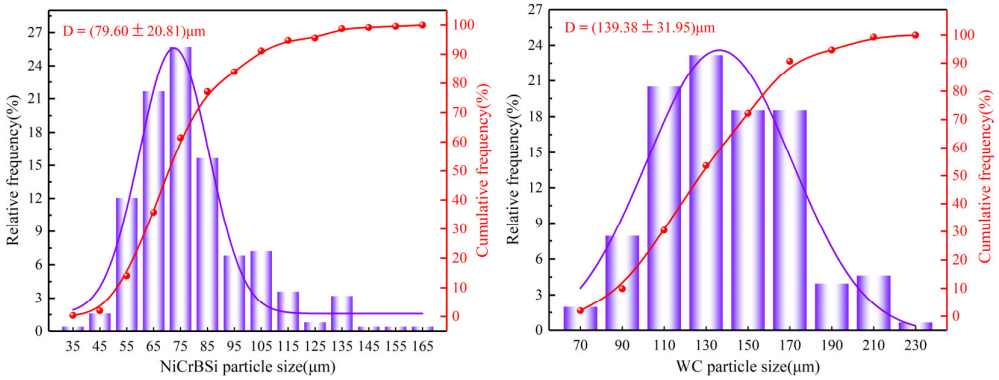

Figure 4. Statistical particle size results of NiCrBSi powder and WC powder.

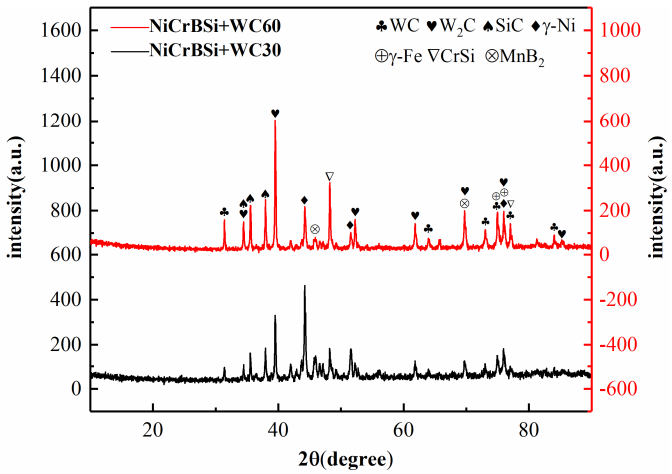

Figure 5. XRD results of alloy powder with different WC additions.

2.2. Experimental Results of Plasma Surfacing Welding

In this study, a DH4-LC401-B12 plasma surfacing mechanism (Duomu Industrial Co., LTD, Shanghai, China) was used to prepare the surfacing layer. Before the welding, the matrix surface was polished with sandpaper to remove burrs and rust on the surface. Then, the experimental block was preheated, the holding furnace temperature was set at 400 °C, and the holding time was 4 h. The plasma surfacing process has a significant effect on the properties of the surfacing layer. Therefore, it is significant to select the best process parameters to improve the performance of the plasma surfacing layer. After many plasma surfacing welding tests, the optimal process parameters, as shown in Table 5, are finally determined.

Table 5. Process parameters of plasma surfacing welding machine.

Welding Parameter	Values
Welding voltage/V	30
Welding current/A	140
Welding speed/(mm/s)	75
Shielding gas velocity/(L/min)	9~10
Powder feed speed/(g/min)	18~20

The experimental results of plasma surfacing welding are shown in Figure 6. After surfacing, the experimental block was insulated for one hour and finally cooled to room temperature. The purpose of preheating and holding before welding is to prevent large stress differences after welding. After welding, the specimens were successively cut into different test blocks along the surfacing layer via electrical spark wire cutting. A total of eight experimental blocks were prepared by selecting characteristic positions. The number of surfacing layer samples for each powder ratio is 4, respectively. The sections were polished step by step with 200#~2000# sandpaper until there were no obvious scratches. Finally, the test blocks were polished with w2.5 and w1.5 polishing agents combined with P-1 polishing machine until the sections became a mirror. The samples to be observed were corroded with aqua for 7~8 s and then immediately sprayed with anhydrous ethanol and dried with a hair dryer. Finally, SEM, XRD, microhardness, friction, wear, and corrosion tests were carried out.

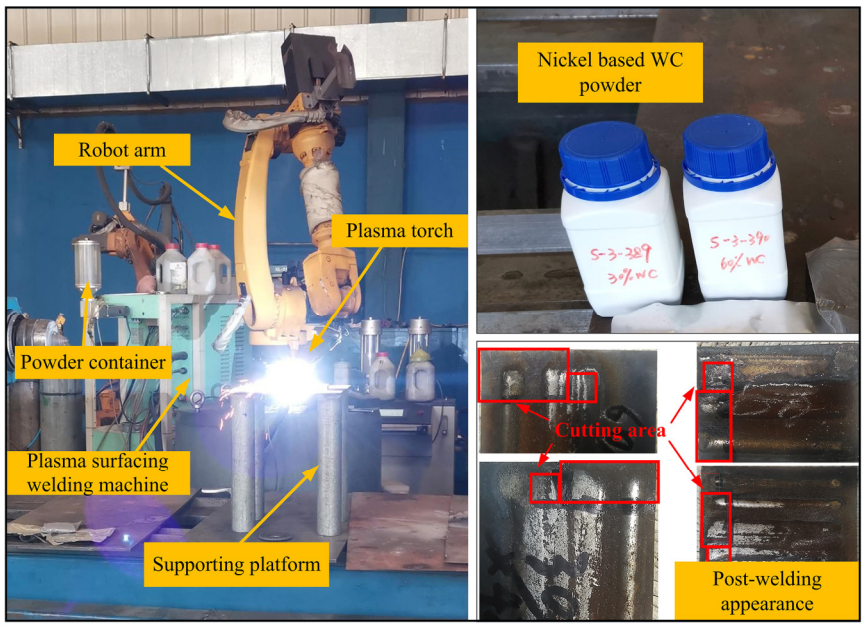

Figure 6. Experimental results of plasma surfacing welding.

3. Analysis of Experimental Results

3.1. Phase Analysis of Surfacing Layer

The phase composition of the surfacing layer has a significant effect on its microstructure and microstructure properties. In this experiment, X'PERT Powder equipment produced by the Panaco Company in the Netherlands was used for the X-ray diffractometer experiment to analyze the phase composition of the surfacing layer. The device uses Kα as the ray source, and the target material is Cu. During the experiment process, the scanning angle was 20°~90° and the scanning time was 2 min. After the experiment is completed, the results are imported into the data processing software to analyze and draw the diffraction curve. Figure 7 shows the XRD test results of the 70%NiCrBSi+30%WC surfacing layer and the 40%NiCrBSi+60%WC surfacing layer. The figure shows that the main phases of the surfacing layer include γ-(Fe/Ni), Fe-Ni, FeSi, Fe_3C, M_7C_3, and other phases, while W_2C, WC, NiCrFe, and other phases are also characterized. The appearance of M_7C_3 and W_2C means that the diffusion and precipitation of elements occur in the weld pool. Among them, the WC particles in the nickel-based WC alloy will dissolve at the edge under the action of heat generated via plasma arc, and the dissolved W and C elements will diffuse into the molten pool and combine with the Cr element in the molten pool to form Cr_7C_3 and other phases. The generation of secondary phases will increase the hardness and wear resistance of the surfacing layer, but a large number of secondary phases will increase the possibility of cracking in the surfacing layer. Figure 7 shows that the phase composition of the surfacing layer obtained by surfacing nickel-based alloys with different WC content does not change, but the content of each phase is significantly different, and the peak value of the WC phase of the 70%NiCrBSi+30%WC surfacing layer is smaller than that of the 40%NiCrBSi+60%WC surfacing layer. When the addition of WC increased from 30% to 60%, the diffraction intensity of the main diffraction peak was obviously changed due to the increase in WC particles and secondary phases in the coating.

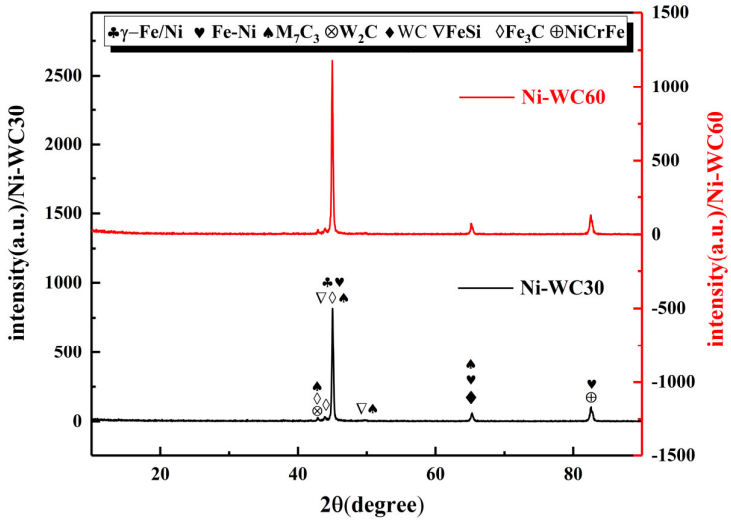

Figure 7. XRD test results of 70%NiCrBSi+30%WC surfacing layer and 40%NiCrBSi+60%WC surfacing layer.

3.2. Analysis of Microstructure Morphology

The content and distribution of WC hard phase in the surfacing layer have a significant influence on the surfacing welding performance. Due to the different WC contents in the plasma surfacing powder raw material, there are obvious differences in the microstructure and hard phase in the surfacing layer. It is necessary to observe the microstructure of the surfacing layer. The microstructure of the 70%NiCrBSi+30%WC surfacing layer is shown in Figure 8. At the position near the fusion line, WC particles are significantly deposited because the density of WC is much higher than that of the nickel-based alloy melt, the melting point of WC is higher, and it will not be completely dissolved even under the

condition of higher heat source energy input. Therefore, in the molten pool composed of WC particles and melted nickel-based alloys, the dense WC particles tend to deposit to the bottom of the molten pool and distribute in the bottom area near the fusion line after solidification, resulting in almost no WC particles at the top of the surfacing layer. The WC particle size at the top of the surfacing layer is smaller than that at the bottom because the WC particles at the top are more affected by the heat of the plasma arc, and the WC particles at the top dissolve at the edge under the high temperature of the plasma arc heat source. Compared with the WC particles at the lower layer, the WC particles at the upper layer experience more serious edge dissolution, and some WC with smaller particle size completely melt and decompose. The dissolution of WC in the molten pool can be carried out via Equations (1)–(3) [22,23]:

$$WC \rightarrow [W] + [C], \quad (1)$$

$$2[W] + [C] \rightarrow W_2C, \quad (2)$$

$$W_2C \rightarrow 2[W] + [C] \quad (3)$$

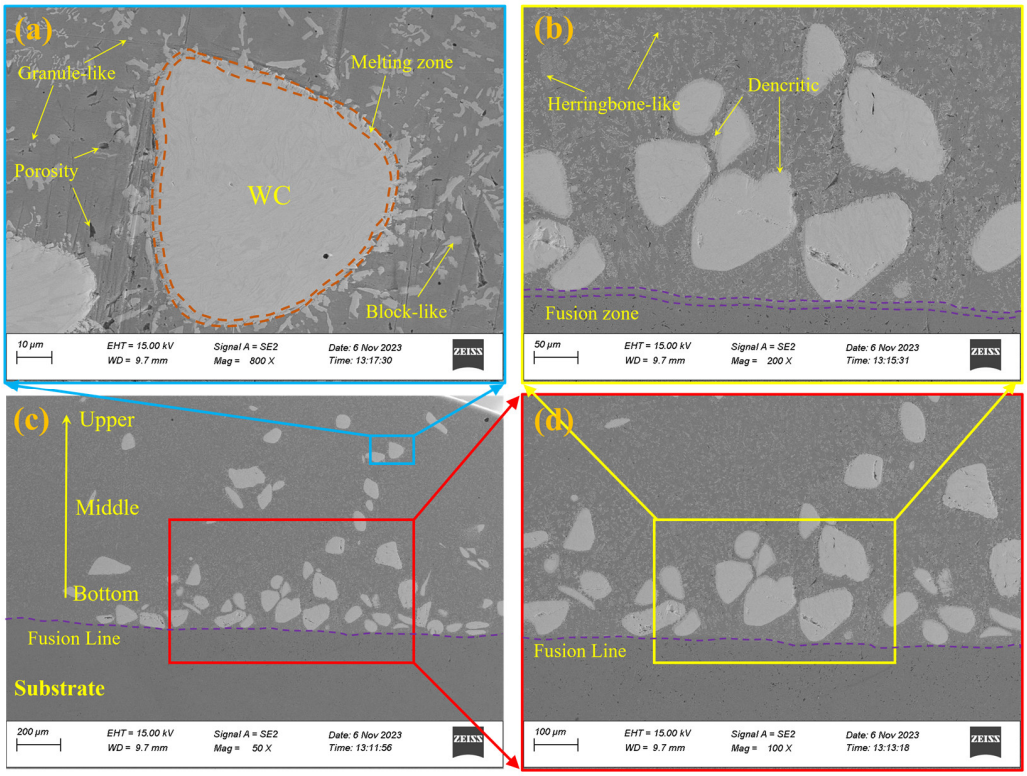

Figure 8. Microtopography of 70%NiCrBSi+30%WC surfacing layer section: (**a**) 800 times; (**b**) 200 times; (**c**) 50 times; (**d**) 100 times.

There is a white bright band at the fusion line of the surfacing layer in Figure 8, which is formed by the mutual diffusion of the molten matrix surface and the alloy liquid phase of the surfacing layer, indicating that the surfacing layer and the matrix have a great metallurgical combination.

The microstructure of the 40%NiCrBSi+60%WC surfacing layer is shown in Figure 9. Compared with the 70%NiCrBSi+30%WC surfacing layer, the deposition of WC particles has been significantly improved. The distribution of WC particles in the surfacing layer is more uniform, no obvious deposition phenomenon occurs, and WC can be observed on the top of the surfacing layer. WC deposition has improved because on the one hand, during the surfacing welding of the 40%NiCrBSi+60%WC powder, the dissolution and diffusion of the W and C elements in the molten pool have significantly increased, and the dissolved

W and C elements enter the nickel-based alloy melt, increasing the melt density of the molten pool, and at the edge of WC, the decomposed W and C elements form new eutectic structures with other elements in the molten pool. These eutectic structures are dendritic and grow radially around WC particles, and the surface of the WC particles becomes very irregular, resulting in the slowing down of WC in the sinking process. On the other hand, in other parts of the molten pool, some W and C elements are diffused into the molten pool under the action of Marangoni flow, forming complex secondary carbides, such as the flake, block, and fishbone, with other alloying elements in the molten pool, which are evenly distributed in the molten pool and are significantly more numerous than the secondary carbides formed by the surfacing welding 70%NiCrBSi+30%WC powder. The precipitation and formation of secondary carbides are also among of the factors that hinder the sinking movement of WC particles. Figure 9 shows that the porosity of the 40%NiCrBSi+60%WC surfacing layer is more than that of the 70%NiCrBSi+30%WC surfacing layer. The reason is that the presence of WC affects the solidification and contraction in the coating and ultimately leads to the pore formations.

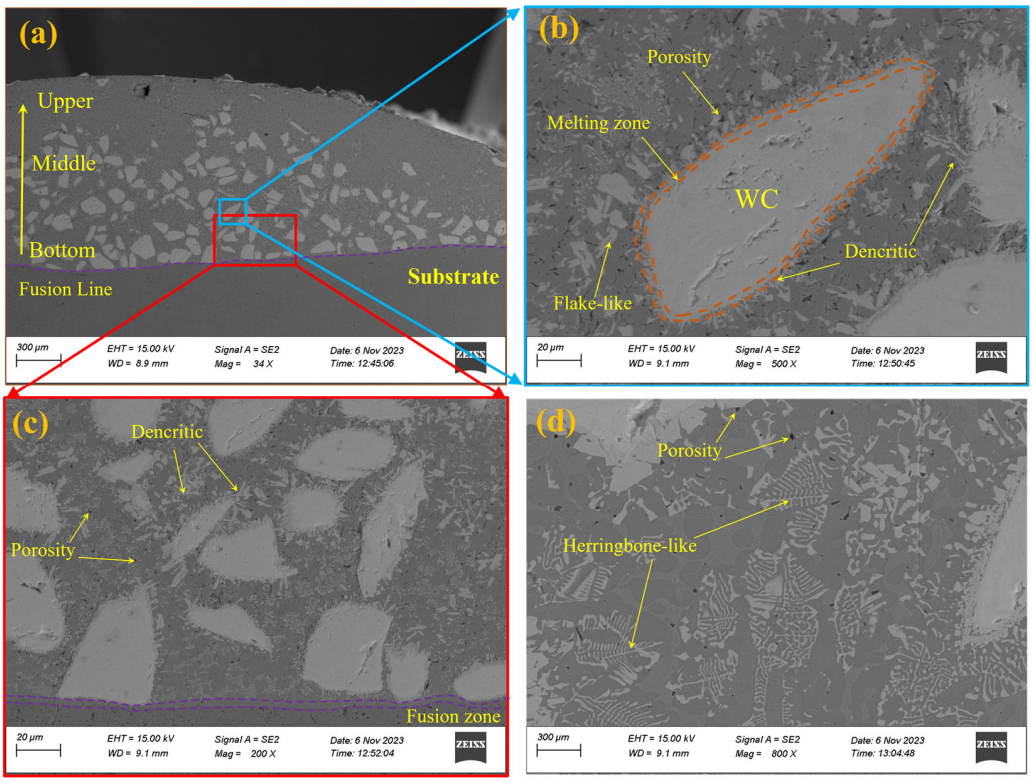

Figure 9. Microstructure of 40%NiCrBSi+60%WC surfacing layer section: (**a**) 34 times; (**b**) 500 times; (**c**) 200 times; (**d**) 800 times.

Figure 10 shows the results of energy spectrum surface scanning in the plasma surfacing layer. As seen in Figure 10, under the action of high heat input of the plasma arc, the edge of the WC particles with high melting point engages in a process of melting–solution–diffusion–precipitation, and the W and C elements decomposed by the WC particles will dissolve and diffuse into the liquid phase of the nickel-based alloy. Ni, Cr, B, Fe, and other elements in the nickel-based alloy will be diffused from the liquid phase nickel-based alloy to the WC particles. The C element is evenly distributed in the nickel-based alloy and the WC particles, and the Cr element is evenly distributed, but the irregular carbides precipitated around the WC particles are concentrated, and the W, Ni, and Fe elements are also concentrated. Therefore, Cr-Fe-Ni-W and a small amount of C can be obtained as the main elements of the new precipitated phase in the nickel-based alloy. Fe and Ni elements are mainly distributed in the surfacing layer and form an Fe-Ni solid solution

together. Different forms of tissue communities were also observed at different positions of the alloy surfacing layer, all containing W element, which was formed for the reaction between the decomposed WC and the elements in the matrix. Due to the different cooling rates at different positions, the diffusion rates of each element were also different, resulting in different contents of W element and other elements in each tissue.

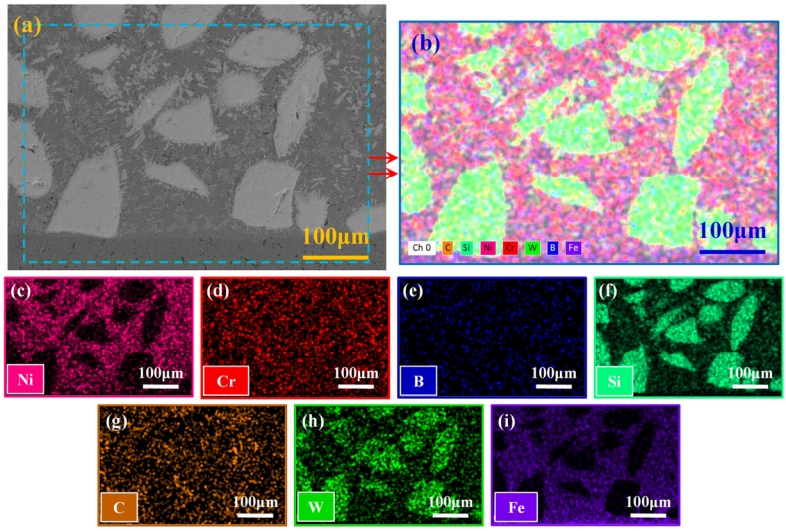

Figure 10. Surface scanning results of the energy spectrum in the surfacing layer: (**a**) 100-fold SEM results in the surfacing layer; (**b**) the element surface scanning results. (**c**–**i**) in the corresponding figure (**a**) are the EDS element surface scanning results of Ni, Cr, B, Si, C, W, and Fe of the corresponding view (**b**).

The microstructure of the WC core, WC edge secondary carbide, and nickel-based alloy in the surfacing welding layer were analyzed via electron probe point scanning, and the results are shown in Figure 11 and Table 6. The electron probe point 1 is the WC particle core, which is mainly composed of W and C elements without other impurity elements. This shows that the composition of the undissolved WC core does not change under the action of the plasma arc heat source. The electron probe point 2 is a nickel-based alloy, and the results are that the main component is an Fe-Ni solid solution with a small amount of Cr, B, and Si elements in solid solution. The electron probe point 3 is a secondary carbide that grows radioactive at the edge of the WC. The point scanning results show that its main components are W, Ni, Fe, and B, and that it contains fewer C, Cr, and Si elements. The analysis results show that there are three types of carbides in the WC hard phase reinforced nickel-based composite surfacing layer. The first type is the undissolved WC particles during surfacing, and the second type is the W and C elements dissolved at the edge of WC particles combine with the elements in the nickel-based alloy to form a secondary carbide at the edge of WC particles. The form of the carbide is different from the original WC. The third type is carbides precipitated by solid solution W, Cr, Ni and other alloying elements at a distance from WC particles.

During the plasma surfacing process, the dissolution behavior of the WC particles has a crucial effect on the structure and properties of the surfacing layer, so it is significant to study the dissolution mechanism of the WC particles. The analysis shows that there are two dissolution mechanisms of the WC particles: one is partial dissolution at the edge of the WC particles; the other is the complete dissolution of the WC particles, and secondary carbides are precipitated again during the solidification process. The partial dissolution mechanism of the WC particles is shown in Figure 12a. Under the action of high-temperature plasma arc, the edges and corners of the irregular WC particles are greatly affected by the heat source; then, a dissolved region is formed around the WC particles, and the W and C elements generated by the dissolution and the elements in the Ni liquid are diffused with each other, and a visible diffusion region is formed around the irregular WC particles. During the molten pool solidification process, a large number of secondary carbides were

precipitated around WC, and some of them were attached to WC particles. At this time, the Ni-based WC surfacing layer was composed of a Ni-based matrix structure, original WC particles, and precipitated secondary carbides. The mechanism of the complete dissolution of the WC particles is shown in Figure 12b. The WC particles in the high heating power area are completely dissolved, and they flow with the melt in the melt pool in the form of W and C elements. Among them, part of the W and C elements reaggregate together, and after solidification, they are re-synthesized into WC particles. Because the plasma arc surfacing welding process is a non-equilibrium metallurgical process, it has the characteristics of urgent heating and cooling, and the rest of the W and C elements solidify without time to gather, forming secondary carbides. However, the melting point of the Ni-based alloy solution is lower than that of WC, and it is still flowing in the melt state. At this time, the Ni-based WC surfacing layer is composed of regenerated WC particles, secondary carbides, and Ni-based matrix structures. The results show that the WC dissolution behavior has no effect on the final structure composition of the surfacing layer, but the spatial distribution of each structure in the surfacing layer significantly changes.

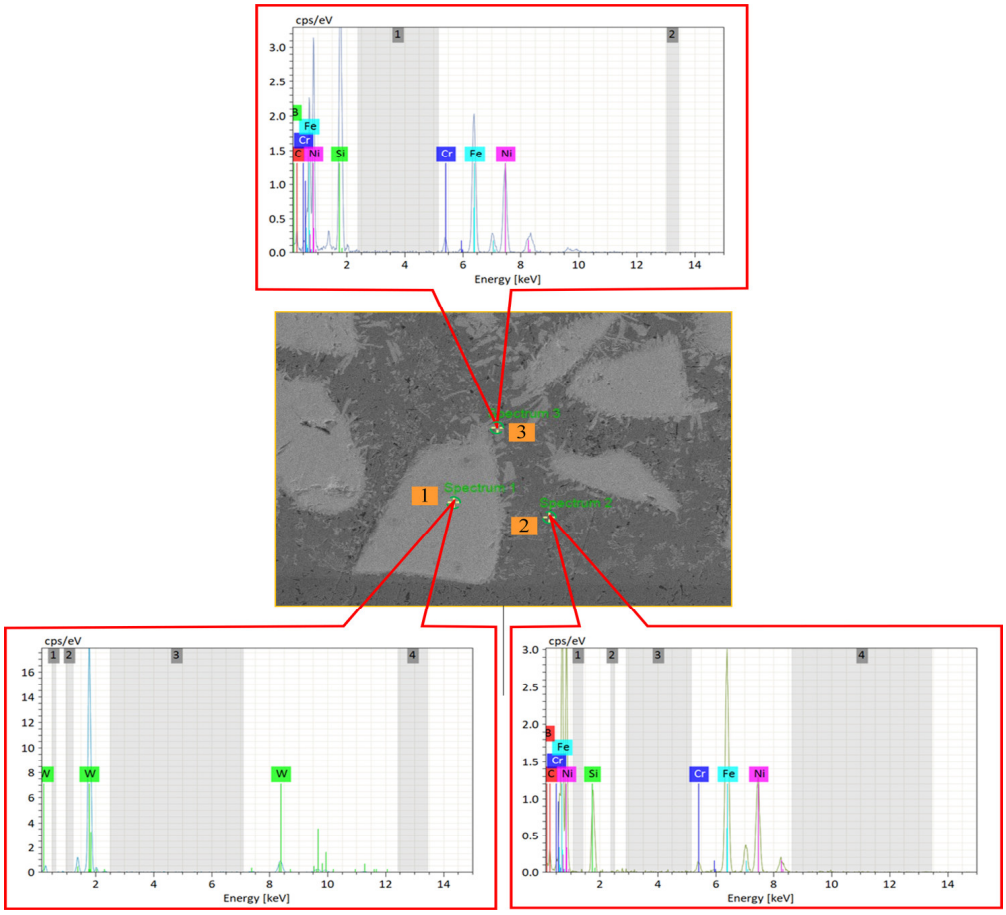

Figure 11. Coating point scan results.

Table 6. Scanning results (atomic percentage) (at%).

Spot	W	C	Ni	Cr	B	Si	Fe
1	94.88	5.12	0.00	0.00	0.00	0.00	0.00
2	0.00	0.00	36.49	1.37	12.13	2.61	47.40
3	22.17	4.24	31.83	1.87	7.06	1.99	30.84

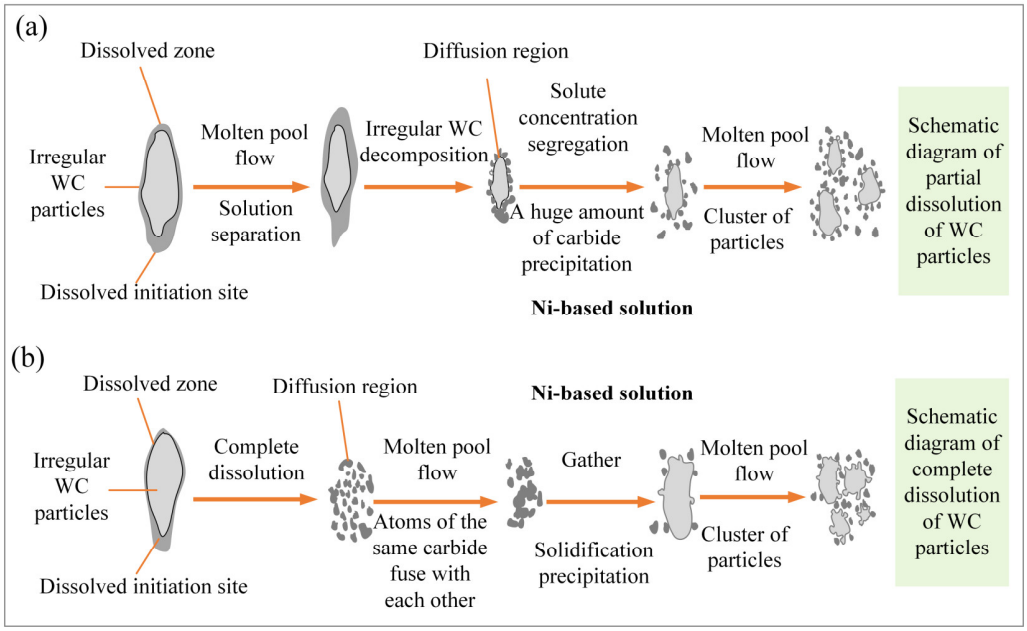

Figure 12. Schematic of WC particle dissolution behavior: (**a**) partial dissolution; (**b**) complete dissolution.

3.3. Microhardness Test

Adding WC as a hard phase to nickel-based alloy powder for plasma surfacing can significantly improve the hardness of the surfacing layer, and the different amounts of WC will have a significant impact on the microhardness. In this paper, a Q10M microhardness tester produced by the QNESS Company in Austria was used to test the hardness of the hard phase and the bonding phase in the matrix and surfacing layer, respectively. Fifteen hardness points were randomly pressed on the 70%NiCrBSi+30%WC surfacing layer and the 40%NiCrBSi+60%WC surfacing layer, in which the matrix, bonding phase, and hard phase had five hardness points each. The load is 3 N, the loading time is 15 s, and the indentation is diamond-shaped. After the hardness test, the hardness indentation morphology was observed with a VHX-500F ultra-depth-of-field microscope produced by the Japan Keenz Company (Keenz Company, Osaka, Japan). Figure 13 shows the statistical diagram of the hardness measurement results. The results show that the hardness of the 42CrMo matrix is about 200 HV, and the hardness of the surfacing layer is obviously higher than that of matrix. Among them, due to the uneven distribution of the newly generated secondary carbides after the decomposition of the WC hard phase, the hardness value of the bond phase fluctuates. In the 70%NiCrBSi+30%WC surfacing layer, the adhesive phase hardness fluctuates up and down at 403.94 HV, while in the 40%NiCrBSi+60%WC surfacing layer, the adhesive phase hardness fluctuates up and down at 485.76 HV. The results show that during the surfacing process, the W and C elements generated by the dissolution of WC edge will diffuse into the surfacing layer to form secondary carbides, and the appearance of these phases can cause secondary phase strengthening and increase the hardness of the surfacing layer. The SEM revealed that with the increase in WC particle content in the surfacing powder, the secondary carbide content increases, which increases the hardness of the bonding phase in the surfacing layer. Figure 13 shows that the hardness of the surfacing layer is significantly higher than that of the matrix, and the hardness of the adhesive phase alone has reached more than 2.5 times that of the matrix, and the hardness of the WC hard phase is higher than 1400 HV. The practice shows that the hardness test is one of the significant evaluation criteria for evaluating the quality of the surfacing layer. The microhardness test shows that plasma surfacing nickel-based WC powder can effectively improve the material surface hardness.

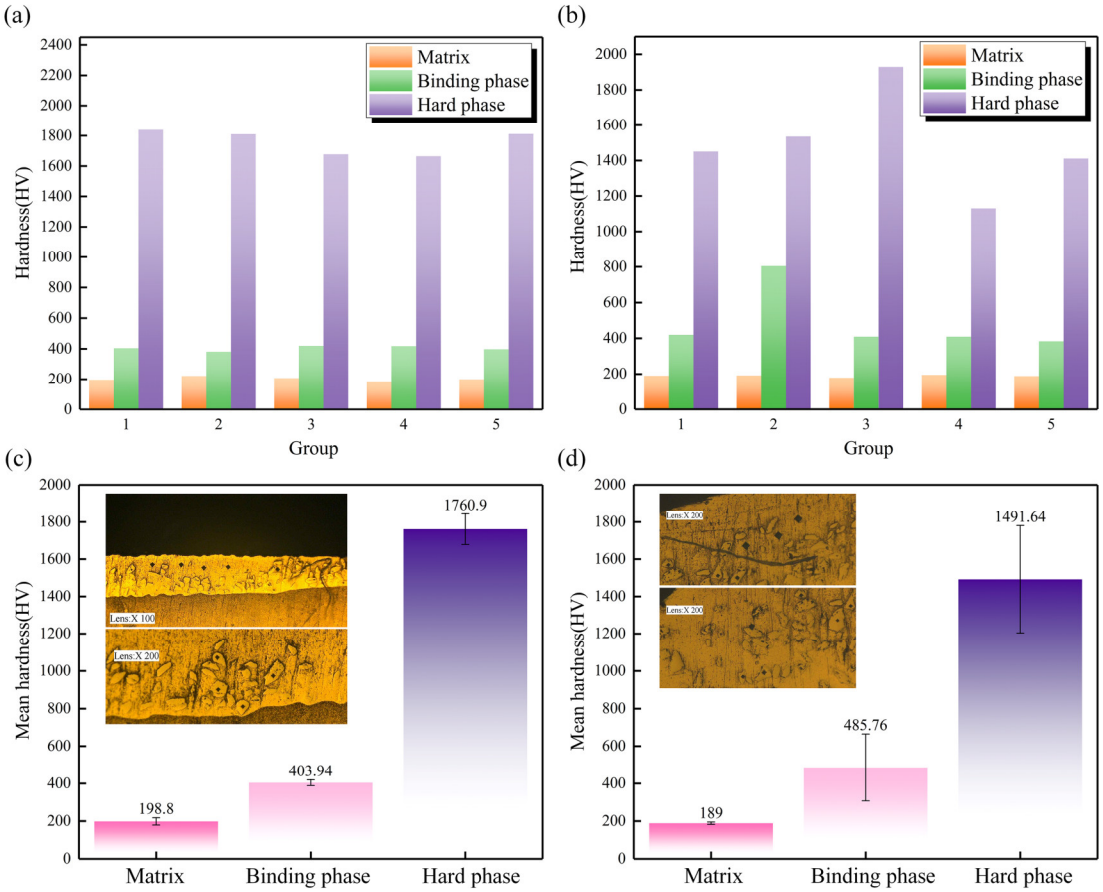

Figure 13. Statistical diagram of hardness results: (**a**) microhardness statistics of the 70%NiCrBSi+30%WC surfacing layer; (**b**) microhardness statistics of the 40%NiCrBSi+60%WC surfacing layer; (**c**) average microhardness statistics of the 70%NiCrBSi+30%WC Surfacing layer; (**d**) statistical results of average microhardness of the 40%NiCrBSi+60%WC surfacing layer.

3.4. Research on Friction and Wear Performance

The excellent wear performance of the surfacing layer on the descaling roller surface is a significant index by which to evaluate its normal service in the high-load and high-wear environment. Therefore, the friction and wear test of the surfacing layer was carried out. The friction and wear testing machine produced by the China Huahui Company was used in the experiment, and the instrument model was MS-T300. Because the addition of WC hard phase particles leads to high wear resistance of the surfacing layer, to accurately test the wear resistance in the surfacing layer, the grinding ball material is Si_3N_4, which has high hardness, as well as has lubricity and wear resistance. In the experiment, the load applied is 1000 g, the wear time is 50 min, the measuring radius is 3 mm, the rotating speed is 300 r/min, and the friction coefficient curve is drawn. After the experiment, the wear marks and the wear of the surfacing layer were observed via an ultra-depth microscope. Under normal circumstances, the smaller the friction coefficient, the better the lubricity of the grinding material under this wear condition. We selected four of the eight experimental blocks prepared, among which there were two experimental blocks with each powder ratio. Each experimental block was subjected to a friction and wear test, and the experimental results with the best effect among each powder ratio experimental block were selected for curve drawing. Figure 14 shows the change curve of the friction and wear coefficient in the surfacing layer. At the beginning of friction, the friction coefficient of the surfacing layer continues to increase because there is a certain amount of oxide on the surface of the surfacing layer in the early friction stage, which has low hardness and a low friction coefficient and belongs to the initial stage of friction (running-in stage). The

friction coefficient in the middle and late period of the friction gradually becomes stable, which belongs to the stable wear stage. Within 0~20 min, the friction coefficient of the 70%NiCrBSi+30%WC surfacing layer first increased and then decreased, and the maximum friction coefficient was 0.31. After 20 min, the friction coefficient of the surfacing layer tended to be stable. During the friction and wear test process, the average friction coefficient was 0.25. Within 0~20 min, the friction coefficient of the 40%NiCrBSi+60%WC surfacing layer gradually increased, and the maximum friction coefficient was 0.29. After 20 min, the friction coefficient of the surfacing layer also tended to be stable, and the average friction coefficient was 0.24. The experimental results show that the wear resistance of the 60%WC surfacing layer is better than that of the 30%WC surfacing layer. The reason is that with the increase in WC content, the number of WC particles in the surfacing layer increases and gradually disperses, and the number of other carbides, borides, and other hard phases in the surfacing layer also correspondingly increases, which improves the hardness of the surfacing layer and also increases the wear resistance. Studies have shown that the hardness of materials has a certain linear relationship with its wear resistance. The higher the hardness of materials, the better the wear resistance [24]. The results of friction and wear test in this study are consistent with the hardness results.

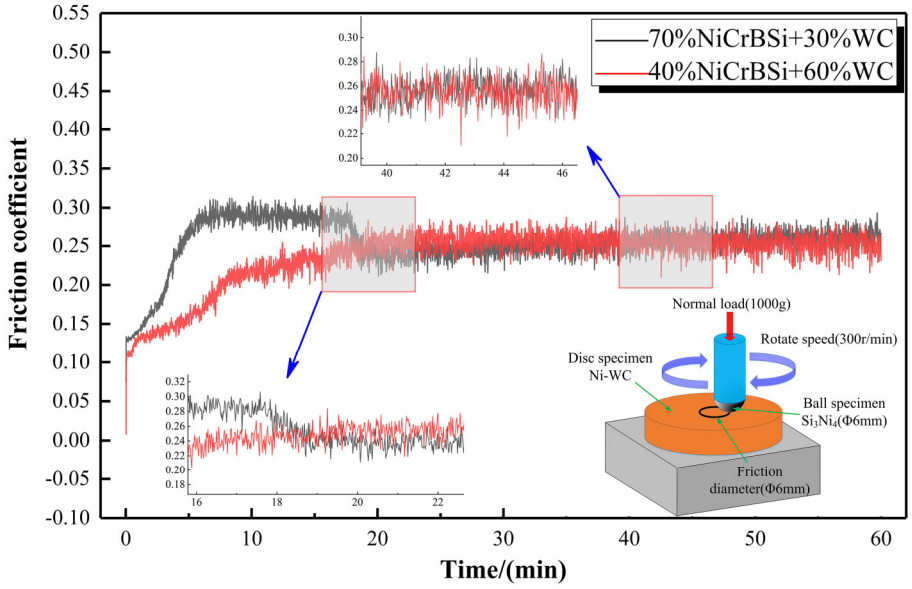

Figure 14. Variation curve of friction coefficient in the surfacing layer.

The wear morphology of the surfacing layers with different WC contents is shown in Figure 15. The abrasion marks are clearly visible under the ultra-depth field microscope. Figure 15a,c show that when the WC content in powder is 30%, the surfacing layer presents obvious wear marks. When the WC content increased to 60%, the abrasion marks significantly narrowed. Due to the hardness and wear resistance of the nickel matrix in the coating being much lower than that of the secondary carbide and the hard phase, the surface nickel matrix is preferentially worn under the action of the grinding material; then, the hard phase such, as the carbide on the surface and sub-surface of the surfacing layer, is gradually exposed, playing the role of a wear-resistant skeleton to reduce the further loss of the nickel matrix. Due to its high toughness, the nickel matrix structure plays a role in supporting the WC particles, reducing the peeling of hard phases such as carbide, and finally improving the wear resistance in the surfacing layer. Therefore, it can be concluded that the wear resistance of the 70%NiCrBSi+30%WC surfacing layer is less than that of the 40%NiCrBSi+60%WC surfacing layer. Figure 15b,d show that a large area of flaky surfacing layer falls off and forms wear marks. Under cyclic contact stress, the surfacing layer forms pits due to the fatigue spalling of materials, resulting in surface shedding. The main wear mechanism of the surfacing layer is surface fatigue wear.

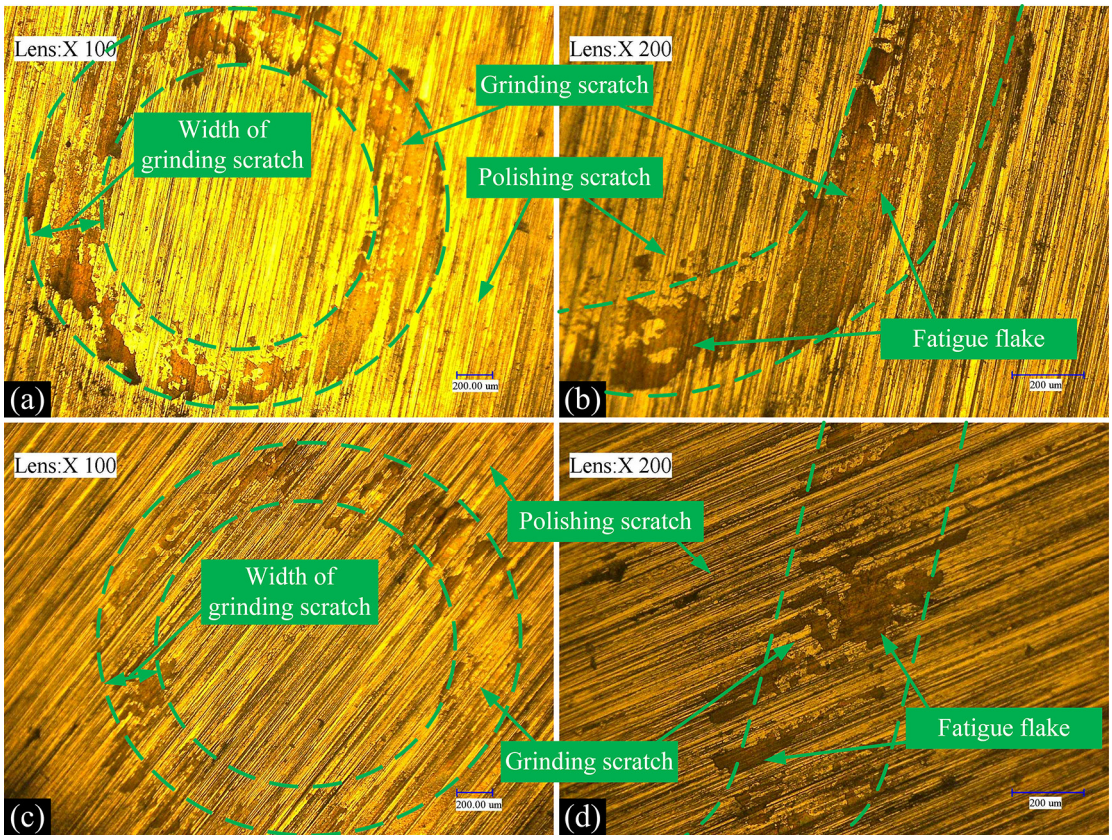

Figure 15. Wear morphology of plasma surfacing layer: (**a**) 70%NiCrBSi+30%WC surfacing layer 100-fold wear morphology; (**b**) 70%NiCrBSi+30%WC surfacing layer 200-fold wear morphology; (**c**) 40%NiCrBSi+60%WC surfacing layer 100-fold wear morphology; (**d**) 40%NiCrBSi+60%WC surfacing layer 200 times wear morphology.

3.5. Analysis of Electrochemical Corrosion Experimental Results

Electrochemical corrosion experiments were carried out on the surfacing layer with the equipment of the Coster CS310M electrochemical workstation (Wuhan Koster Instrument Co., LTD, Wuhan, China) at room temperature, with 3.5% NaCl solution as the corrosion solution. The 3.5% NaCl solution was prepared using NaCl dissolved in deionized water, and the NaCl was produced by the Shenyang Dongxing reagent factory (Shenyang Dongxing reagent factory, Shenyang, China) (purity: 99.5%). The working electrode was the test block, the reference electrode was saturated with calomel, and the auxiliary electrode was platinum sheet. The initial scanning point was −0.2 V, and the scanning termination potential was 1.2 V. The scanning speed is 0.16 mV/s. Before the test, the parts not involved in the test are encapsulated and dried with epoxy resin, and only the surfacing layer under test is exposed to the corrosion solution. To accurately evaluate the corrosion resistance of the surfacing layer, 304 stainless steel with high corrosion resistance was selected for comparative analysis. Figure 16 shows the polarization curves of 304 stainless steel with the 70%NiCrBSi+30%WC surfacing layer and the 40%NiCrBSi+60%WC surfacing layer, where the horizontal coordinate is the corrosion current (I) and the vertical coordinate is the corrosion potential (E). To evaluate the degree of corrosion, self-corrosion potential and self-corrosion current density were calculated via the Tafel extrapolation method to characterize the degree of corrosion. The calculation results are shown in Table 7. Among them, the self-corrosion current density of 304 stainless steel is 1.79×10^{-10} A/cm^2, the self-corrosion potential is −0.23 V, and the corrosion rate is 2.10×10^{-6} mm/a. The criterion of electrochemical kinetics is that the lower the self-corrosion current density, the slower the corrosion rate [25,26]. The electrochemical thermodynamic criterion is that the more positive the self-corrosion potential, the stronger the corrosion resistance [27,28].

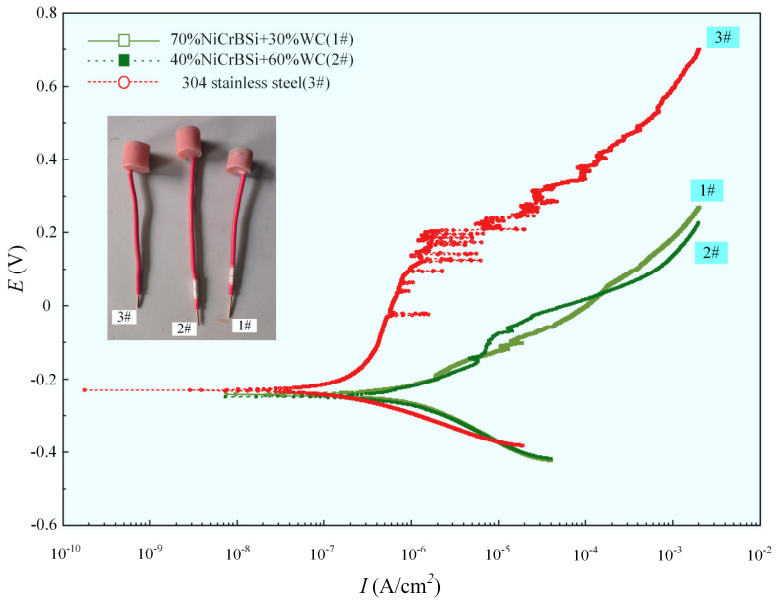

Figure 16. Polarization curves of 304 stainless steel with the 70%NiCrBSi+30%WC surfacing layer and the 40%NiCrBSi+60%WC surfacing layer.

Table 7. Results of electrochemical experiments.

Number	Self-Corrosion Current Density *I*/(Amps/cm^2)	Self-Corrosion Potential *E*/(Volts)	Self-Corrosion Rate/(mm/a)
304 stainless steel	1.79×10^{-10}	−0.23	2.10×10^{-6}
70%NiCrBSi + 30%WC surfacing layer	4.51×10^{-7}	−0.24	5.29×10^{-3}
40%NiCrBSi + 60%WC surfacing layer	7.36×10^{-9}	−0.25	8.63×10^{-5}

Through the data comparison of the self-corrosion rate, the corrosion resistance can be obviously compared. The self-corrosion rate of the 70%NiCrBi+30%WC surfacing layer is 5.29×10^{-3} mm/a, and the self-corrosion rate of the 40%NiCrBi+60%WC surfacing layer is 8.63×10^{-5} mm/a. The corrosion resistance of the 70%NiCrBi+30%WC surfacing layer is less than the corrosion resistance of the 40%NiCrBSi+60%WC surfacing layer, which is because WC itself has great corrosion resistance, and its main component, tungsten, has high chemical stability and can resist the erosion of many chemical media. A surfacing layer with more WC added has better corrosion resistance. By comparison, it can also be found that the corrosion resistance of the 40%NiCrBSi+60%WC surfacing layer is less different from that of 304 stainless steel. For 304 stainless steel, the positive self-corrosion potential indicates that it has great corrosion resistance, and the low self-corrosion current density also reflects its slow corrosion rate under specific conditions, which is consistent with the characteristics of 304 stainless steel as a corrosion-resistant material, verifying the accuracy and reliability of the electrochemical corrosion experiment results.

4. Conclusions

In this paper, 70%NiCrBSi+30%WC powder and 40%NiCrBSi+60%WC powder were used as surfacing materials; plasma surfacing experiments were carried out on 42CrMo matrix; and SEM, XRD, microhardness, friction, and wear and corrosion tests were carried out on the surfacing layer to evaluate the feasibility of preparing an ultra-high-hardness WC-particle-reinforced nickel-based alloy plasma surfacing layer on the descaling roller surface and to explore the WC hard phase dissolution behavior and complex secondary phase formation mechanism. Based on welding tests, this study revealed the correlation between the powder formula, welding structure, and surfacing layer properties. The main conclusions are as follows:

(1) The XRD results of the surfacing layer show that the Ni/WC plasma surfacing layer mainly consists of γ-(Fe/Ni), Fe-Ni, FeSi, Fe_3C, M_7C_3, and other phases, while W_2C, WC, NiCrFe, and other phases are also characterized. The appearance of M_7C_3 and W_2C means that the diffusion and precipitation of elements occur in the weld pool. The diffraction peaks of the surfacing layers with different WC contents are obviously different, but the phase composition of the surfacing layer does not change.

(2) Compared with the 70%NiCrBSi+30%WC surfacing layer, the WC deposition phenomenon of the 40%NiCrBSi+60%WC surfacing layer is significantly improved. Due to the WC addition increase and the WC edge dissolution, more complex secondary phases are generated and precipitated, and the surfacing layer has better hardness and wear resistance. The main wear mechanism of the surfacing layer is surface fatigue wear.

(3) The dissolution mechanism of the WC particles is divided into partial dissolution and complete dissolution. No matter the kind of dissolution mechanism, the Ni-based WC surfacing layer is composed of WC particles, secondary carbides, and Ni-based matrix. The results show that the WC dissolution behavior has no effect on the final structure composition of the surfacing layer, but the spatial distribution of each structure changes on the surfacing layer.

(4) There are three types of carbides in the WC hard phase reinforced nickel-based composite surfacing layer. The first type is the undissolved WC particles during surfacing, and the second type is the W and C elements dissolved at the edge of WC particles combine with the elements in the nickel-based alloy to form a secondary carbide at the edge of WC particles. The third type is carbides precipitated by solid solution W, Cr, Ni and other alloying elements at a distance from WC particles.

(5) Electrochemical corrosion experiments show that the corrosion resistance of the 70%NiCrBSi+30%WC surfacing layer is less than that of the 40%NiCrBSi+60%WC surfacing layer. Among them, the corrosion resistance of the 40%NiCrBSi+60%WC surfacing layer makes little difference with 304 stainless steel.

Author Contributions: Methodology, H.S.; Investigation, L.F., X.H. and F.L.; Resources, C.L.; Writing—original draft, L.F.; Writing—review & editing, L.F.; Supervision, C.L., X.H. and F.L. All authors have read and agreed to the published version of the manuscript.

Funding: This work was supported by The Ministry of Science and Technology of the People's Republic of China under the project "High-Throughput Design, Preparation, and Characterization of Composite Powders for Special Coatings on Key Components in Metallurgy" (2021YFB3702002); The Applied Basic Research Project of Liaoning Province (2023JH2/101300226); The Project for Graduate Education Reform and Technological Innovation and Entrepreneurship of the University of Science and Technology Liaoning (2023YJSCX02).

Institutional Review Board Statement: Not applicable.

Informed Consent Statement: Not applicable.

Data Availability Statement: The data that supports the findings of this study are available within the article.

Conflicts of Interest: The authors declare no conflict of interest.

References

1. Pohanka, M.; Votavová, H.; Resl, O.; Kotrbáček, P. The Effect of Water Jet Overlaps in a Descaler on the Quality of Surface of the Hot Rolled Steel. *Metals* **2023**, *13*, 1722. [CrossRef]
2. Gongye, F.; Zhou, J.; Peng, J.; Zhang, H.; Peng, S.; Li, S.; Deng, H. Study on the Removal of Oxide Scale Formed on 300 M Steel Special-Shaped Hot Forging Surfaces during Heating at Elevated Temperature by a High-Pressure Water Descaling Process. *Materials* **2023**, *16*, 1745. [CrossRef] [PubMed]
3. Appiah, A.N.; Wyględacz, B.; Matus, K.; Reimann, Ł.; Bialas, O.; Batalha, G.F.; Czupryński, A.; Adamiak, M. Microstructure and performance of NiCrBSi coatings prepared by modulated arc currents using powder plasma transferred arc welding technology. *Appl. Surf. Sci.* **2024**, *648*, 159065. [CrossRef]
4. Li, N.; Wang, Q.; Dong, F.; Liu, X.; Han, P.; Han, Y. Research progress of coating preparation on light alloys in aviation field: A review. *Materials* **2022**, *15*, 8535. [CrossRef] [PubMed]

5. Sun, S.; Wang, J.; Xu, J.; Cheng, X.; Jing, C.; Chen, Z.; Ru, H.; Liu, Y.; Jiao, J. Preparing WC-Ni coatings with laser cladding technology: A review. *Mater. Today Commun.* **2023**, *37*, 106939. [CrossRef]
6. Deenadayalan, K.; Murali, V. Role of various weight percentages of WC particle on interface thickness and friction-wear property of NiCrBSi-WC composite fabricated using PTAW process. *Mater. Res. Express* **2019**, *6*, 046542. [CrossRef]
7. Farias, F.W.; da Cruz Payão Filho, J.; da Silva Júnior, D.A.; de Moura, R.N.; Rios, M.C. Microstructural characterization of Ni-based superalloy 625 clad welded on a 9% Ni steel pipe by plasma powder transferred arc. *Surf. Coat. Technol.* **2019**, *374*, 1024–1037. [CrossRef]
8. Sudha, C.; Shankar, P.; Rao, R.S.; Thirumurugesan, R.; Vijayalakshmi, M.; Raj, B. Microchemical and microstructural studies in a PTA weld overlay of Ni–Cr–Si–B alloy on AISI 304L stainless steel. *Surf. Coat. Technol.* **2008**, *202*, 2103–2112. [CrossRef]
9. Kesavan, D.; Kamaraj, M. The microstructure and high temperature wear performance of a nickel base hardfaced coating. *Surf. Coat. Technol.* **2010**, *204*, 4034–4043. [CrossRef]
10. Sreevidya, N.; Rani, R.; Das, C.R.; Mathews, T.; Albert, S.K.; Vasudevan, M.; Ramaseshan, R. Effect of Dilution on High-Temperature and High-Vacuum Tribological Behaviour of Ni-Cr-B-Si Hardfaced Coating. *Trans. Indian Inst. Met.* **2023**, *76*, 3127–3136. [CrossRef]
11. Kumar, H.; Mishra, R.K.; Harmain, G.A.U. Effect of mating material on wear behaviour of Ni-based hardface coating. *Proc. Inst. Mech. Eng. Part L J. Mater. Des. Appl.* **2024**, *238*, 481–492. [CrossRef]
12. Zhao, P.; Shi, Z.; Wang, X.; Li, Y.; Cao, Z.; Zhao, M.; Liang, J. A Review of the Laser Cladding of Metal-Based Alloys, Ceramic-Reinforced Composites, Amorphous Alloys, and High-Entropy Alloys on Aluminum Alloys. *Lubricants* **2023**, *11*, 482. [CrossRef]
13. Shen, X.; Peng, H.; Xue, Y.; Wang, B.; Su, G.; Zhu, J.; Li, A. Microstructure and Properties of WC/Ni-Based Laser-Clad Coatings with Different WC Content Values. *Materials* **2022**, *15*, 6309. [CrossRef] [PubMed]
14. Perrin, T.; Achache, S.; Meausoone, P.J.; Sanchette, F. Characterization of WC-doped NiCrBSi coatings deposited by Laser Cladding effects of particle size and content of WC powder. *Surf. Coat. Technol.* **2021**, *425*, 17460–17470. [CrossRef]
15. Zhang, X.; Dong, M.; Cai, X.; Chen, D.; Xian, Y.; Zheng, X.; Guo, Z.; Algadi, H. Progress in machining-induced residual stress and microstructural evolution of inhomogeneous materials and composites. *Adv. Compos. Hybrid Mater.* **2023**, *6*, 122. [CrossRef]
16. Yan, Y.F.; Kou, S.Q.; Yang, H.Y.; Shu, S.L.; Qiu, F.; Jiang, Q.C.; Zhang, L.C. Ceramic particles reinforced copper matrix composites manufactured by advanced powder metallurgy: Preparation, performance, and mechanisms. *Int. J. Extrem. Manuf.* **2023**, *5*, 032006. [CrossRef]
17. Ying, W.E.; Wei, X.S.; Bo, C.H.; Zuo, J.Y.; Jun, S.H. Parameter optimization for tungsten carbide/Ni-based composite coating deposited by plasma transferred arc hardfacing. *Trans. Nonferrous Met. Soc. China* **2018**, *28*, 2511–2519.
18. Wang, W.; Zeng, X.; Li, Y.; Wang, D.; Liu, Y.; Yamaguchi, T.; Nishio, K.; Cao, J. Fabrication, microstructure, and wear performance of WC-Fe composite/metal coating fabricated by properties seam welding. *Mater. Charact.* **2017**, *134*, 182–193. [CrossRef]
19. Appiah, A.N.; Bialas, O.; Czupryński, A.; Adamiak, M. Powder Plasma Transferred Arc Welding of Ni-Si-B+60wt%WC and Ni-Cr-Si-B+45wt%WC for Surface Cladding of Structural Steel. *Materials* **2022**, *15*, 4956. [CrossRef]
20. Adamiak, M.; Appiah, A.N.; Żelazny, R.; Batalha, G.F.; Czupryński, A. Experimental comparison of laser cladding and powder plasma transferred arc welding methods for depositing wear-resistant NiSiB+60% WC composite on a structural-steel matrix. *Materials* **2023**, *16*, 3912. [CrossRef]
21. Yi, J.; Niu, B.; Pan, L.; Zou, X.; Cao, Y.; Wang, X.; Luo, J.; Hu, Y. Influence of WC grain size on the microstructure and wear property enhancement of 18Ni300 coatings. *Surf. Coat. Technol.* **2022**, *447*, 128823. [CrossRef]
22. Zafar, S.; Sharma, A.K. Structure-property correlations in nanostructured WC–12Co microwave clad. *Appl. Surf. Sci.* **2016**, *370*, 92–101. [CrossRef]
23. Sundaramoorthy, R.; Tong, S.X.; Parekh, D.; Subramanian, C. Effect of matrix chemistry and WC types on the performance of Ni-WC based MMC overlays deposited by plasma transferred arc (PTA) welding. *Wear* **2017**, *376*, 1720–1727. [CrossRef]
24. Da, D.Q.; Gong, Y.L.; Xiao, Q.T. Microstructure and properties of laser cladding Ni-alloy and Co-alloy on the Surface of Cr12MoV mould steel. *Hot Work. Technol.* **2004**, *8*, 49–51.
25. Ciubotariu, C.R.; Frunzaverde, D.; Marginean, G. Investigations of Cavitation Erosion and Corrosion Behavior of Flame-Sprayed NiCrBSi/WC-12Co Composite Coatings. *Materials* **2022**, *15*, 2943. [CrossRef]
26. Xiao, J.K.; Wu, Y.Q.; Zhang, W.; Chen, J.; Wei, X.L.; Zhang, C. Microstructure, wear and corrosion behaviors of plasma sprayed NiCrBSi-Zr coating. *Surf. Coat. Technol.* **2019**, *360*, 172–180. [CrossRef]
27. Sabzi, M.; Dezfuli, S.M.; Mirsaeedghazi, S.M. The effect of pulse-reverse electroplating bath temperature on the wear/corrosion response of Ni-Co/tungsten carbide nanocomposite coating during layer deposition. *Ceram. Int.* **2018**, *44*, 19492–19504. [CrossRef]
28. Zeng, Q.; Sun, J.; Emori, W.; Jiang, S.L. Corrosion behavior of thermally sprayed NiCrBSi coating on 16MnR low-alloy steel in KOH solution. *J. Mater. Eng. Perform.* **2016**, *25*, 1773–1780. [CrossRef]